Journal of Solid State Chemistry 183 (2010) 795–802

Contents lists available at ScienceDirect

Journal of Solid State Chemistry

journal homepage: www.elsevier.com/locate/jssc

Interactions between Eu^{3+} ions in inorganic–organic hybrid materials

Fabienne Pellé [a,*], Patrick Aschehoug [a], Suzy Surblé [b], Franck Millange [c], Christian Serre [c], Gérard Férey [c]

[a] Chimie de la Matière Condensée de Paris, UMR 7574 CNRS, Université Pierre et Marie Curie ENSCP, 11 rue Pierre et Marie Curie, 75235 Paris, France
[b] European Commission, Joint Research Centre, Institute for Transuranium Elements, P.O. Box 2340, Karlsruhe 76125, Germany
[c] Institut Lavoisier de Versailles, UMR 8180 CNRS, Université de Versailles St-Quentin en Yvelines, 45 Avenue des Etats-Unis, 78035 Versailles Cedex, France

ARTICLE INFO

Article history:
Received 25 November 2009
Received in revised form
21 January 2010
Accepted 27 January 2010
Available online 2 February 2010

Keyword:
Hybrid materials
Optical properties
Upconversion

ABSTRACT

The optical properties of two-dimensional lanthanide dicarboxylates EuBDC or $Eu_2(H_2O)_2(O_2C–C_6H_4–CO_2)_3$ and EuCDC (denoted also MIL94) or $Eu_2(H_2O)_4(O_2C–C_6H_{10}–CO_2)_3.2H_2O$ are reported. The structures are built up from dimers of corner-sharing polyhedra and 1,3-benzenedicarboxylate (BDC) for EuBDC and from dimers of edge-sharing polyhedra and 1,3-benzenedicarboxylate (CDC) for EuCDC. The high Eu^{3+} concentration and the weak luminescence quenching allow the study of Eu^{3+} interactions. Anti-Stokes spectra from $^5D_1$ are observed with excitation in $^5D_0$. These results are very unusual for Eu^{3+} ions and reflect strong interactions between ions within a dimer. Excitation spectrum of the Eu^{3+} luminescence strongly differs in both compounds in the UV range. In case of EuBDC, an efficient sensitization of the luminescence due to the ligand is observed between 250 and 350 nm while only 4f–4f transitions are recorded on the Eu^{3+} excitation spectrum in EuCDC. The efficiency of the sensitization of the rare earth by the host is discussed by taking into account the geometrical arrangement and the electronic delocalization of the ligands.

1. Introduction

A growing interest in lanthanides complexes and inorganic–organic hybrid materials has aroused in the last few years and the researches in this field are mainly focused on efficient light converting devices. As a matter of fact, the trivalent rare earth ions (RE) are characterized by narrow emission lines that are suitable for photonic applications. However, the 4f–4f transition probabilities are very weak to achieve efficient light converters. So, it is necessary to sensitize the RE by strong absorbing species able to transfer efficiently their excitation energy to the emitting centers. Such efficient energy transfer from organic ligands to RE ions was demonstrated [1] and the so-called "antenna effect" proposed by Lehn [2] was shown to be a powerful strategy to populate efficiently the RE^{3+} excited states and to overcome the 4f–4f small absorption coefficients. This opened the way to realize efficient UV light converters using new concepts of rare earth doped materials for photonic applications. A wide panel of applications is concerned, for example in biology with time resolved fluoroimmunoassays [3–5], protein conformational changes [6], determination of DNA [7], electroluminescent displays [8,9] and UV dosimetry [10]. In this regard, the design of efficient UV light converter devices based on RE-complexes or hybrid inorganic–organic compounds is very topical. Main studies are devoted to Ln-complexes and a great number of organic ligands (chelates, cryptates, calix-arenes, etc.) have already been considered [11]. A correlation between the lowest triplet state energy level of the organic part and Ln^{3+} luminescence quantum yield of complexes has been established for a wide panel of ligands [12] and energy transfer ligand-Ln^{3+} modelised [13]. Recently we have considered in a systematic way the effect of the inorganic skeleton, i.e. RE polyhedra arrangement and the nature of the organic part in organic–inorganic hybrid materials [14–18] on the optical properties. These materials have been also widely studied owing to their interesting properties for other purposes like magnetism, gas separation, catalysis and hydrogen storage [19–22].

In this paper, we have focused our interest on the optical properties of two layered lanthanide carboxylates EuBDC and EuCDC. Their two dimensional structure can be described as chains of dimers related to the dicarboxylate anions. The structures of EuBDC and EuCDC have been recently described and the Eu^{3+} fluorescence spectrum was briefly reported [23,24]. We have extended the synthesis to Tb^{3+} and Gd^{3+} and mixed Gd^{3+}/Eu^{3+} based materials in order to identify the excitation band observed in the UV range.

Here, we have studied more in-depth the Eu^{3+} optical properties, especially interactions between Eu^{3+} within dimers, and have tried to demonstrate the influence of the electronic delocalization in the ligand: 1,3-benzenedicarboxylate (BDC) for EuBDC versus 1,3-cyclohexanedicarboxylate (CDC) on the Eu^{3+} sensitization. Therefore, an optical study of Eu^{3+} ions in both

* Corresponding author.
E-mail address: fabienne-pelle@chimie-paristech.fr (F. Pellé).

0022-4596/$ - see front matter © 2010 Elsevier Inc. All rights reserved.
doi:10.1016/j.jssc.2010.01.028

structures has been conducted with high spectral and temporal resolution. Energy transfer between Eu^{3+} ions is demonstrated and strong interactions between dimers are evidenced from the observation of upconversion fluorescence of $^5D_1$ state to the ^7F_J multiplets with excitation in the $^5D_0$ level for both compounds. Such upconversion process in Eu^{3+}doped material is extremely rare and to our knowledge has only been observed twice in inorganic materials [25,26]. However, if the 4f–4f (Eu^{3+}) transitions are very similar, the Eu^{3+} excitation spectra differ for both materials in the UV range. This will be discussed based on the nature of the ligands, which determines the efficiency of the ligand–rare earth energy transfer.

2. Experimental

2.1. Synthesis and structure

EuBDC or $Eu_2(H_2O)_2(O_2C–C_6H_4–CO_2)_3$ and EuCDC or $Eu_2(H_2O)_4(O_2C–C_6H_{10}–CO_2)_3\cdot 2H_2O$ were hydrothermally synthesized at 493 K from a mixture of rare-earth nitrate $Eu(NO_3)_3\cdot 5H_2O$ (Aldrich, 98%), 1,3-benzenedicarboxylic acid (Aldrich, 99%) or 1,3-cyclohexanedicarboxylic acid (Aldrich, 99%), respectively, sodium hydroxide NaOH (Prolabo, 99%) and H_2O in the molar ratio 1:1.5:1.5–2:180. In a last step, the synthesis was repeated to obtain the pure rare earth forms of EuBDC and EuCDC (Ln∼Gd, Tb, Gd-doped Eu 2% and 5%) using similar synthesis conditions.

These solids exhibit a two dimensional structure, which are built up from dimers of europium polyhedra, linked by the 1,3-benzenedicarboxlate or 1,3-cyclohexanedicarboxylate groups. Europium atoms are seven and eight coordinated in EuBDC surrounded by six or seven oxygen atoms from the carboxylates groups and one terminal water molecule per cation. In the case of EuCDC, lanthanide cations are nine-coordinated with seven oxygen atoms from the organics and two terminal water molecules per cation. The mode of connection within the rare earth dimers is different in the two solids as shown in Fig. 1; in EuBDC, this is a corner sharing mode while in EuCDC, polyhedra are sharing edges. Complete details on synthesis and structure analysis have been already published [24].

2.2. Spectroscopy

The fluorescence, excited by an optical parametric oscillator (OPO) pumped by the third harmonic of a Thales Q-switched Nd:YAG laser or directly by the third harmonic for UV excitation, was dispersed and analyzed by a ICCD Roper scientific camera (intensified charge coupled device) coupled to an HR 25 Jobin–Yvon monochromator, for low resolution measurements. Detection was assured by a Jobin–Yvon CCD-3500V coupled to an HR460 Jobin–Yvon monochromator for higher resolution measurements. Low temperature measurements were performed by cooling the samples in a closed-cycle CTI cryogenic cryostat.

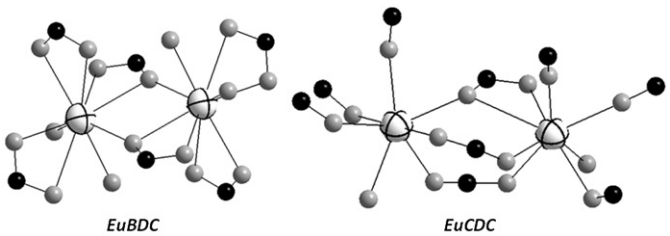

Fig. 1. Dimer structure and connecting mode dicarboxylates–europium ions in EuBDC and EuCDC. Europium, carbon and oxygen atoms are represented, respectively, in white (with black ellipse, black and grey).

The excitation spectra were performed using the radiation provided by a 150 W XBO Xenon lamp dispersed by a HD20 Jobin–Yvon monochromator, the luminescence analyzed through an HR1000 Jobin–Yvon monochromator and detected by an RTC 56 TVP photomultiplier and amplified by a PAR 128a lock-in amplifier with data acquisition on a microcomputer. The data were corrected from the response of the acquisition device.

3. Results: spectroscopic properties

3.1. UV excitation

Rare earth doped materials are usually excited in the UV range, and then emission spectra of the different materials were recorded at room temperature under excitation at 355 nm. In the series of Eu^{3+} materials based on 1,3-benzenedicarboxylic acid (BDC), emission spectra are similar to the Eu^{3+} concentration and only the spectrum of EuBDC is represented in Fig. 2 (curve *a*). The fluorescence spectrum of EuCDC recorded under the same conditions is represented in Fig. 2 (curve *b*).

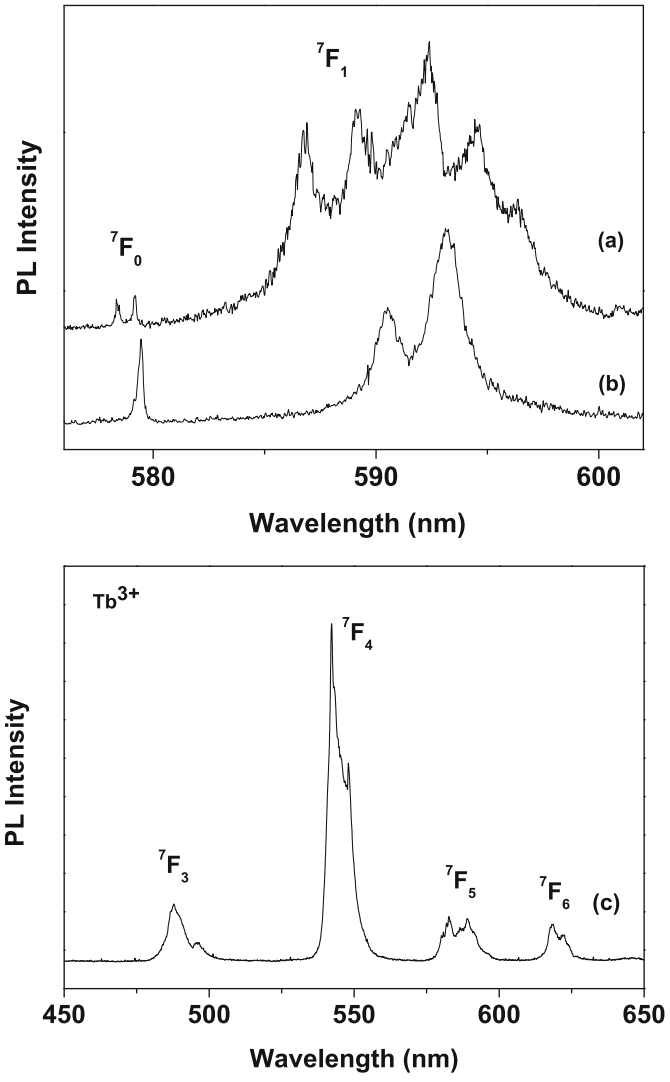

Fig. 2. Luminescence spectrum recorded at room temperature under UV excitation. At 355 nm: (a) EuBDC; (b) EuCDC; (c) TbBDC. The observed transitions arise from the $^5D_0$ states (case of Eu^{3+}, only transitions to $^7F_{0,1}$, which are the most relevant for our purpose, are detailed), $^5D_4$ (case of Tb^{3+}) and the labels refer to the final states.

In both materials EuBDC and EuCDC the fluorescence features observed between 570 and 720 nm are characteristic of $4f^6$–$4f^6$ transitions of Eu^{3+} ion and are easily ascribed to the transitions from the $^5D_0$ state to the lower ^7F_J multiplets (J=0,1,2,3,4). The spectrum is dominated by the $^5D_0 \rightarrow {}^7F_2$ hypersensitive transition. Two and one lines are recorded for the $^5D_0 \rightarrow {}^7F_0$ transition for compounds EuBDC and EuCDC, respectively, in agreement with the crystallographic data. $^5D_0 \rightarrow {}^7F_{0,1}$ transitions are detailed in Fig. 2(a) and (b) since for low J values only a few number of lines are expected, which usually allow easy separation of the different sites. For EuBDC, a great number of lines are observed on the emission spectrum, especially for the $^5D_0 \rightarrow {}^7F_1$ transition, due to the contribution of two Eu^{3+} sites. The complete spectra have already been reported in [24] and are detailed in Figs. 7 and 10 for EuBDC and EuCDC, respectively.

In a similar way, the spectral features observed for TbBDC (or $Tb_2(H_2O)_2(O_2C–C_6H_4–CO_2)_3$) are easily identified to the 4f–4f transitions from the $^5D_4$ state to the ^7F_J multiplets (J=6,5,4,3) as shown in Fig. 2(c).

Excitation spectra performed monitoring the hypersensitive emission $^5D_0 \rightarrow {}^7F_2$ are represented in Fig. 3. In order to make a comparison between EuCDC and EuBDC, the spectra have been normalized to the intensity of the excitation in the magnetic dipolar transition $^7F_0 \rightarrow {}^5D_1$, whose intensity is independent of the environment. In both cases, the spectral features observed between 520 and 300 nm correspond to the excitation process from $^7F_0$ and $^7F_1$ ground states to $^5D_1$, $^5D_2$, $^5D_3$ and $^5L_6$ multiplets. The excitation line intensities recorded for both materials in this spectral range are quite similar. For EuBDC, in addition to the intra-configurational transitions, a broad band is observed between 350 and 240 nm.

The UV excitation band can arise either from a charge transfer Eu^{3+}–O^{2-} or from an energy transfer from the triplet state of the ligand to the rare earth. To answer this question, optical properties of gadolinium based BDC materials GdBDC: Ln^{3+} (Ln^{3+}=Eu^{3+} (2 and 5 at%), Tb^{3+} (2 at%) were investigated. Indeed, the first excited state $^6P_{7/2}$ of Gd^{3+} lies at high energy (>30 000 cm^{-1}) and, in hybrid materials, depending of the relative position of the electronic states of the ligand states with the $^6P_{7/2}$ multiplet, emission from Gd^{3+} or from the ligand are observed under UV excitation. Then, replacing Eu^{3+} or Tb^{3+} by Gd^{3+} allows determining the energies of the electronic states of the ligand as shown already [27].

Emission spectra of the Gd based BDC materials excited at 266 nm are represented in Fig. 4. For pure Gd^{3+} and Eu^{3+} doped GdBDC, a broad emission band is observed between 420 and 600 nm, whose intensity decreases with increase in the Eu^{3+} concentration and disappears in full Eu^{3+} and Tb^{3+} concentrated systems EuBDC and TbBDC, respectively.

On the excitation spectra (Fig. 5), except the lines easily ascribed to the intra-configurational transitions for Eu^{3+} and Tb^{3+}, the band observed in the UV range is the same in all the compounds. Due to the great similarity between the excitation spectra of Eu^{3+} and Tb^{3+} in the UV range, this broad band is ascribed to the electronic transitions within the ligand since charge transfer transition Ln^{3+}–O^{2-} should be observed at different energies going from Eu^{3+} to Tb^{3+}. The UV excitation and the emission bands recorded for Gd based materials lie in the spectral range, which is usually observed for organic ligands [12,27–29]. From these results, the UV excitation band is ascribed

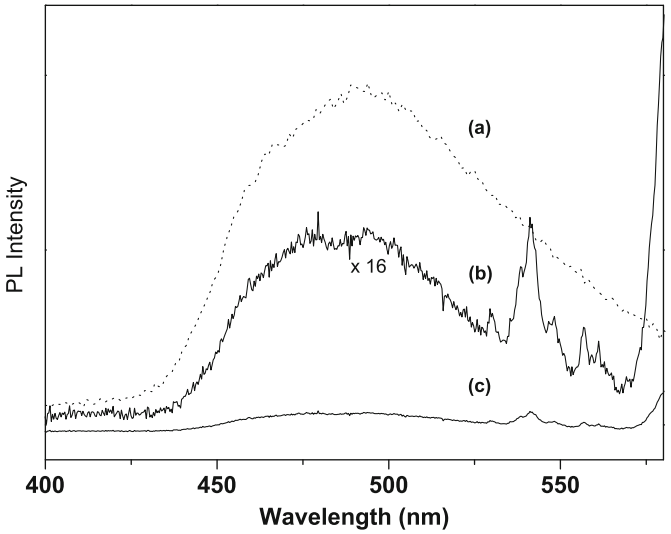

Fig. 4. Luminescence spectrum recorded at room temperature under UV excitation at 266 nm: (a) GdBDC; (b) GdBDC: Eu(2%) (multiplied by a factor 16); (c) GdCDC: Eu(2%).

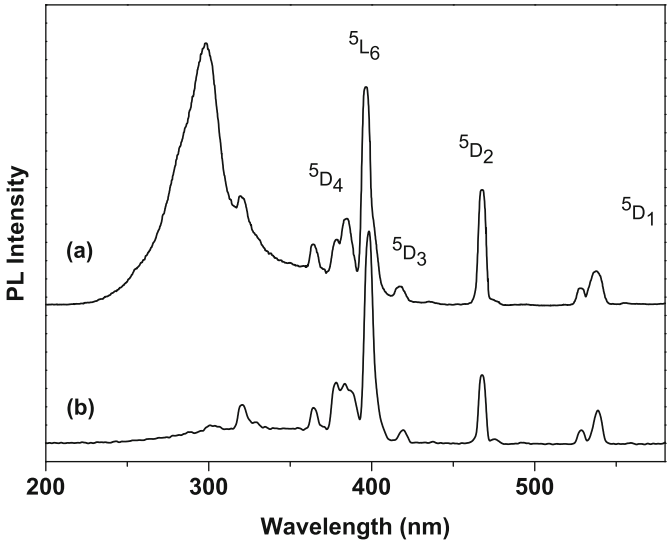

Fig. 3. Excitation spectra monitoring the $^5D_0 \rightarrow {}^7F_2$ transition (a) EuBDC; (b) EuCDC. Data have been normalized to the $^7F_0 \rightarrow {}^5D_1$ intensity (the observed transitions arise from the $^7F_{0,1}$ states, the labels refer to the final states).

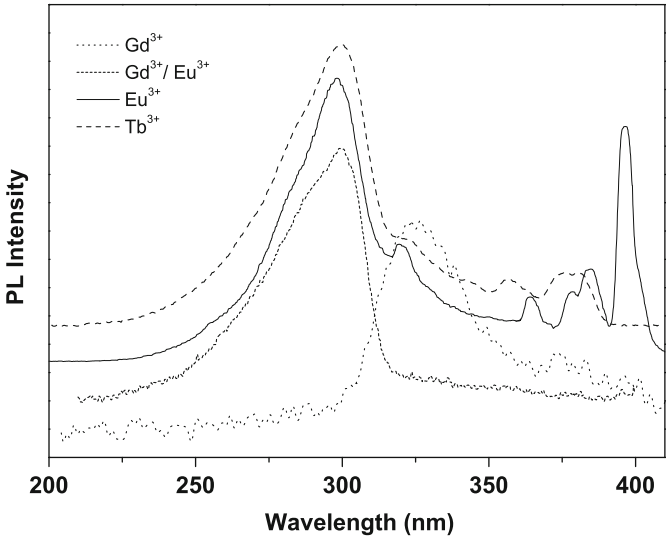

Fig. 5. Excitation spectrum of GdBDC: Eu^{3+} (2%), EuBDC monitoring the $^5D_0 \rightarrow {}^7F_2$ (Eu^{3+}) and GdBDC: Tb^{3+} (2%) monitoring the $^5D_4 \rightarrow {}^7F_6$ transition.

to the electronic transition within the ligand from the ground state ($^1S_0$) to the singlet state ($^1S_1$) while the emission band corresponds to the $^3T_1 \rightarrow {}^1S_0$ transition of the ligand following an inter-crossing system. The ligand electronic states lie at an energy favorable to an efficient energy transfer to the rare earth; this explains the quenching of the $^3T_1$ ligand emission with the introduction of Eu^{3+} or Tb^{3+} ions. The efficiency of the ligand–RE energy transfer observed for EuBDC and the absence of such a transfer in EuCDC will be discussed in Section 4.3.

3.2. Selective excitation and time resolved luminescence spectra

3.2.1. EuBDC

Site selective spectroscopy has been performed on EuBDC using a pulsed tunable laser excitation in order to get emission spectra from Eu^{3+} ions located in the different sites of the structure.

3.2.1.1. Excitation in the $^5D_0$ state. Under selective excitation in both $^5D_0 \rightarrow {}^7F_0$ emission lines at 579.2 nm (site I) and 578.5 nm (site II), respectively, only slight changes are observed at room temperature as a function of the excitation energy in comparison with the spectrum recorded with a non-selective excitation. Emission spectrum from individual sites cannot be recorded independently from each other; for the sake of simplicity only the spectrum recorded after excitation in site I is represented in Fig. 6 (curve *a*).

Lowering the temperature to 10 K, time resolved spectra under selective excitation in both $^5D_0 \rightarrow {}^7F_0$ lines allow separating the emission spectrum related to both sites for a short delay after the excitation pulse (Fig. 6 curves *b*, *c* full lines). However, on the fluorescence spectrum recorded at longer delay, emission lines from both sites are observed (Fig. 6 curves *b*, *c* dotted lines). From the decay profiles recorded at 10 K with selective excitation, a direct energy transfer and a back transfer between site I and site II are already occurring at low temperature, probably because of the low energy difference ($21\ cm^{-1}$) between the $^5D_0$ states and the dimer structure, which favors interactions. The comparison of the fluorescence spectra recorded at 10 and 300 K shows that emission lines from site II are very weak at room temperature irrespective of the excitation. Under excitation in the $^5D_0$ state (site I), the non-exponential behavior of the $^5D_0$ decay, observed at short time, is more pronounced at room temperature than at 10 K as shown in Fig. 9(a). This demonstrates the occurrence of the energy transfer between Eu^{3+} ions as it is expected from the dimer structure of the material and in agreement with the results obtained with a selective excitation in the $^5D_0$ states of Eu^{3+} in both sites as a function of temperature. Sufficient energy is provided by phonons even at low temperature to bridge the very weak energy difference ($21\ cm^{-1}$) between the $^5D_0$ states and allows energy transfer between the two sites at 10 K. The time constant of the exponential part of the decay is reduced with increase in temperature due to the multiphonon relaxation.

Time resolved measurements as a function of temperature with different excitations reveal a complex dynamics for the $^5D_0$ state (site I and site II); the detailed study of the transfer processes between Eu^{3+} ions in this material will be reported in a forthcoming paper.

3.2.1.2. Excitation in the $^5D_1$ and $^5D_2$ states. Time resolved spectra have been recorded with excitation in the $^5D_2$ and $^5D_1$ multiplets. The emission spectra excited in $^5D_2$ and $^5D_1$ states are similar and extend from 520 to 730 nm. Using a very short delay (100 ns) after the excitation pulse and a short gate (1 μs), the emission spectrum differs (Fig. 7 curve *a*) from that represented in Fig. 2 (curve *a*) while the emission spectrum taken at a long delay after the excitation pulse (Fig. 7 curve *b*) allows recording the emission from the $^5D_0$ state as observed in Fig. 2 (curve *a*).

The spectroscopic features observed at short times are ascribed to the transitions from the lower $^5D_1$ component to the ^7F_J (J=0–4) multiplets. This hypothesis is confirmed by plotting emission spectra in energy scale and scaling the origin to the $^5D_1$ and $^5D_0$ energy, respectively. Detailed transitions are represented in Fig. 8. All lines observed at short delay can be assigned to transitions from the $^5D_1$ lowest Stark component to the ^7F_J states.

No line can be identified for emission transition from the $^5D_2$ excited state to the ^7F_J multiplets. Best results are obtained by taking into account for the $^5D_0$ energy for site I whose $^5D_0 \rightarrow {}^7F_0$ transition is observed at 579.2 nm and most of the lines from the $^5D_1$ emitting state to ^7F_J correspond to transitions observed with excitation in $^5D_0$ (I). The time resolved emission spectra obtained with excitation in $^5D_0$ and $^5D_2$ at room temperature are mostly due to the contribution of site I as observed with selective excitation in the $^5D_0$ level of Eu^{3+} in sites I and II.

The temporal behavior of the $^5D_1$ and $^5D_0$ states has been measured with excitation in $^5D_2$ (Fig. 9b). At room temperature,

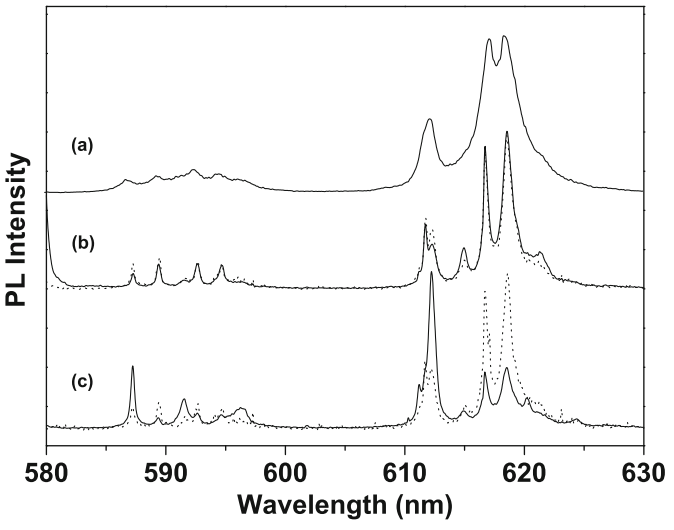

Fig. 6. Luminescence recorded under laser site selective excitation in EuBDC. (a) Excitation in site I (room temperature), (b) excitation in site II (10 K); (c) excitation in site I (10 K) (experimental data: dotted lines; theoretical fit: full lines).

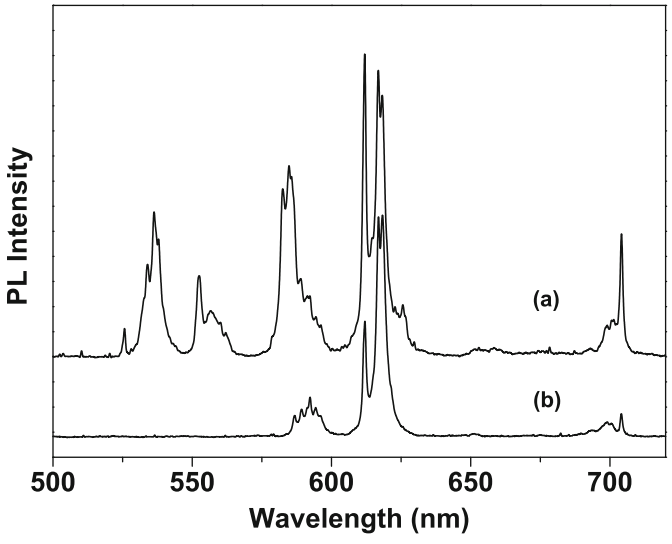

Fig. 7. Luminescence spectrum of EuBDC excited in $^5D_2$ state recorded at room temperature: (a) short delay after the excitation pulse; (b) long delay after the excitation pulse.

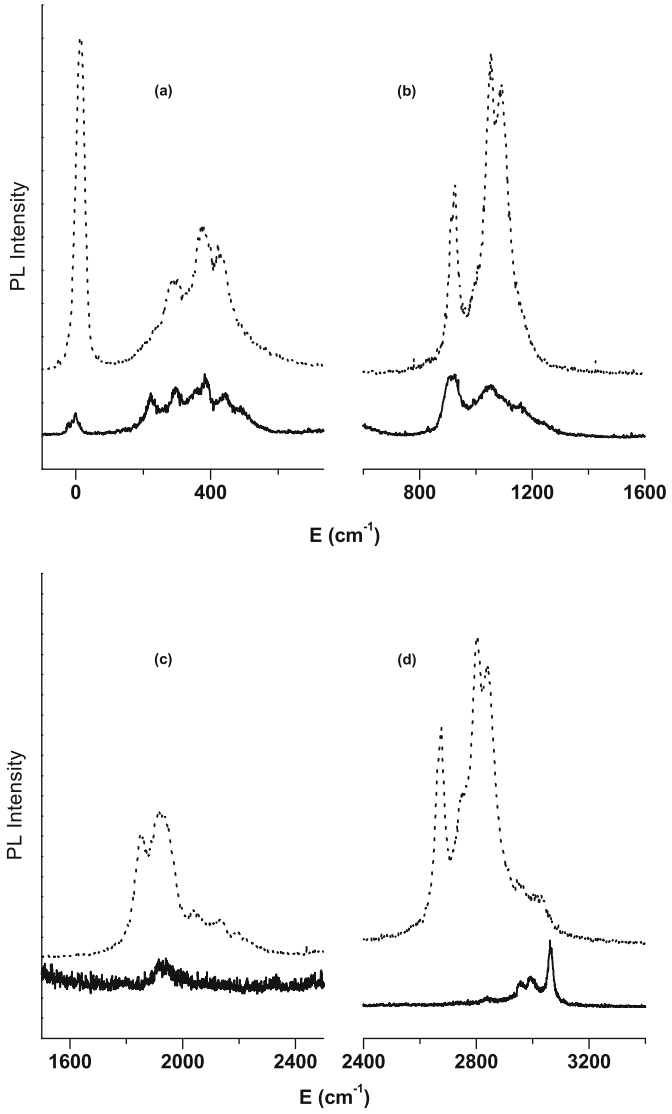

Fig. 8. Energy of the ^7F_J components deduced from the luminescence spectrum of EuBDC excited in $^5D_2$ state at room temperature, (a) $^7F_0$ and $^7F_1$, (b) $^7F_2$, (c) $^7F_3$, (d) $^7F_4$; continuous lines: transitions from $^5D_0$; dotted lines: transitions from $^5D_1$.

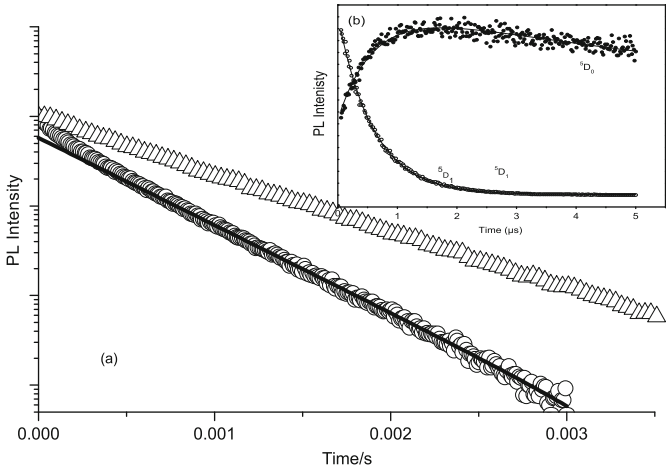

Fig. 9. (a) Transient of the $^5D_0$ state excited in $^5D_0$ (I) recorded at 10 K and at room temperature (symbols: experimental data: triangles for 10 K, circles for RT; continuous lines: theoretical. (b) Transient of the $^5D_0$ and $^5D_1$ states in EuBDC excited in $^5D_2$ (room temperature).

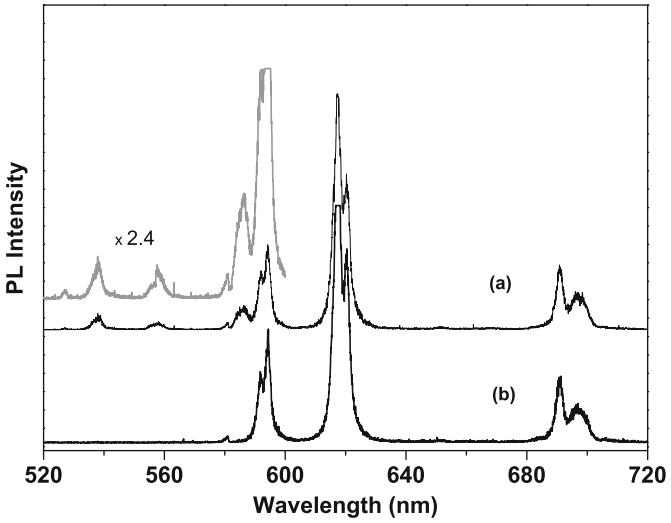

Fig. 10. Luminescence spectrum of EuCDC excited in $^5D_2$ state recorded at room temperature: (a) short delay after the pulse excitation; (b) long delay after the pulse excitation.

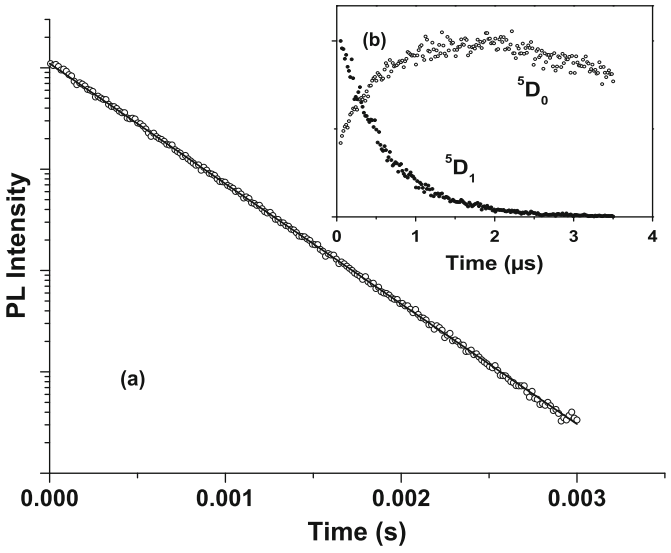

Fig. 11. Transient of the $^5D_0$ state in EuCDC (excitation in $^5D_2$, room temperature).

the $^5D_1$ temporal transient, recorded monitoring the $^5D_1 \rightarrow {}^7F_1$ transition, can be fit with an exponential function, whose time constant equals 596 ns (Fig. 9 continuous line theoretical fit). The intensity of the $^5D_0$ level first increases exponentially with a time constant equal to the lifetime of $^5D_1$ (Fig. 9(b) continuous line theoretical fit). The long part of the decay decreases exponentially with a time constant equal to 410 μs. Emission spectra recorded at short times confirm the previous assignment to the different transitions. From these results, we can conclude that emission from $^5D_2$ is quenched since no emission can be observed from this level. The processes involved in this quenching will be discussed in the following sections.

3.2.2. EuCDC

3.2.2.1. Excitation in the $^5D_1$ and $^5D_2$ states. As in the previous case, pulsed excitation in the $^5D_2$ state gives rise to transitions from $^5D_1$ and $^5D_0$; no emission can be identified to $^5D_2 \rightarrow {}^7F_J$.

Emissions recorded at a short delay (100 ns) after the laser pulse and using a short gate (500 ns) are assigned to $^5D_1$–^7F_J transitions (Fig. 10 curve *a*). Spectral features recorded

with a gate of 1 μs opened 10 μs after the laser pulse are well identified for transitions from the $^5D_0$ level to the ^7F_J multiplets (Fig. 10 curve *b*).

However, the relative intensity of $^5D_1$ emissions and that of $^5D_0$ is much weaker in that case compared to the spectrum recorded with EuBDC under the same conditions. Furthermore, the contrary is observed with EuBDC: only transitions from $^5D_1$ to $^7F_{0,1,2}$ exhibit a significant intensity compared to transitions from $^5D_0$ (Fig. 10 curve *b*). The quenching process for $^5D_2$ and $^5D_1$ multiplets will be proposed and discussed in the following sections.

The decay profiles of $^5D_1$ and $^5D_0$ excited in $^5D_2$ are represented in Fig. 11(b). The intensity of the $^5D_1$ emission decreases with time following an exponential law with a time constant of 588 ns. The emission of $^5D_0$ first increases with a time constant corresponding to the decay of $^5D_1$ and then decreases. Under a direct excitation the $^5D_0$ exhibits a perfect exponential behavior; the measured lifetime is equal to 373 μs (Fig. 11(a)).

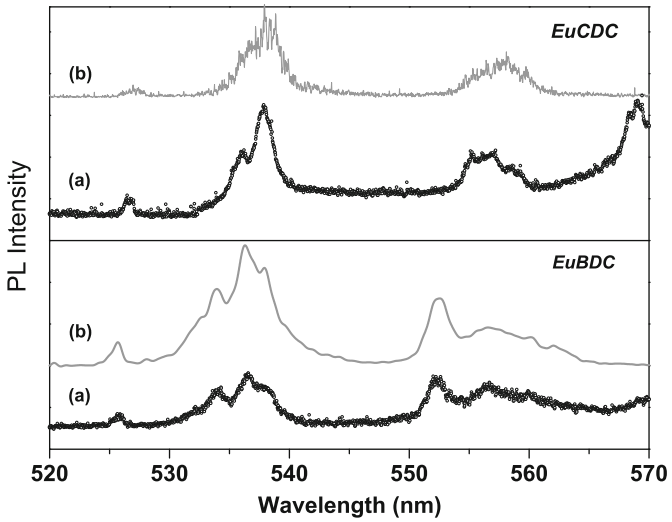

Fig. 12. Stokes and anti-Stokes emissions recorded at room temperature after excitation in $^5D_0$ state: EuBDC: (a) excitation in $^5D_0$ (P=15 mW), (b) excitation in $^5D_2$, EuCDC: (a) excitation in $^5D_0$ (P=15 mW), (b) excitation in $^5D_2$.

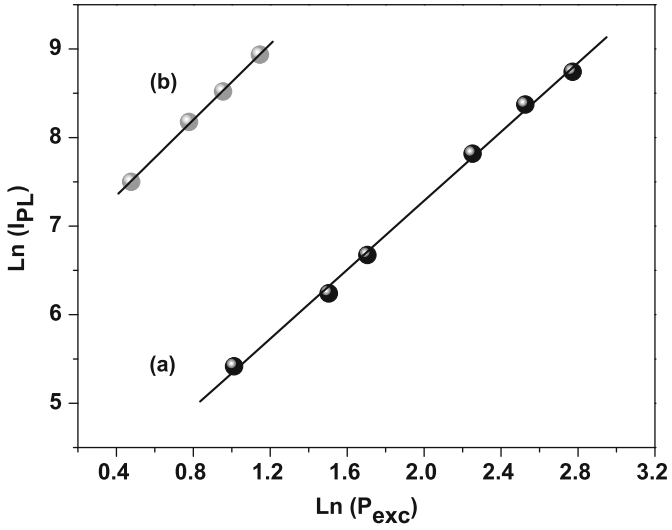

Fig. 13. Integrated intensity of luminescence as a function of excitation power: (a) EuBDC, (b) EuCDC (symbols: experimental data, continuous lines: linear fit).

3.3. Upconversion luminescence spectra

For both compounds, with increase in the excitation power in the $^5D_0$ state, anti-Stokes emissions are observed between 570 and 525 nm as shown in Fig. 12 for EuBDC and EuCDC, respectively. The excitation was set at 579.2 nm (site I) for EuBDC. These anti-Stokes emissions are easily identified to electronic transitions from the $^5D_1$ state from both sites since they are identical to $^5D_1$ Stokes emission as shown in Fig. 12 for EuBDC for EuCDC. The upconverted emission from the $^5D_1$ state exhibits a higher efficiency in EuCDC than when resonantly excited as a result of the quenching of the $^5D_1$ state by cross-relaxation. The quenching processes of the $^5D_1$ state are discussed in Section 4.1.2.

The intensity of these anti-Stokes emissions varies following a quadratic dependence with the excitation power. Linear fit of Ln(I), I being the experimental intensity of the anti-Stokes emission with Ln(P), P being the power of the laser excitation gives slopes equal to 1.95 for EuBDC and 2.13 for EuCDC, respectively (Fig. 13). These results demonstrate the occurrence for a two-photon process giving rise to the observation of anti-Stokes emissions. It is important to note here that very few works have been reported to date on upconversion with Eu^{3+} ions [25,26].

4. Discussion

4.1. Decays

4.1.1. Self-quenching of $^5D_0$

The time constant corresponding to the $^5D_0$ state is found to be very short in both materials compared to other RE carboxylate hybrid materials we have recently studied [14–18]. Then, the presence of water molecules in the first coordination sphere is not sufficient to explain such a reduction. Furthermore, the $^5D_0$ lifetime measured in LnBDC decreases with increase in the Eu^{3+} concentration. The self-quenching of the $^5D_0$ state of Eu^{3+} is still questionable. Contrary to other RE ions, cross-relaxation processes by multipolar transfer processes involving one ion in the $^5D_0$ state and a neighboring ion in its ground state are not possible due to the large energy gap separating $^5D_0$ from the immediately lower state, i.e. the $^7F_6$ multiplet ($\sim$12350 cm^{-1}), which widely exceeds the $^7F_0$–$^7F_6$ energy difference ($\sim$4900 cm^{-1}). To explain a lifetime reduction of the $^5D_0$ state in Eu^{3+} doped materials, exchange and super-exchange interactions have been invoked [30]. These processes can operate in our materials since two neighboring ions are connected by one oxygen ion (EuBDC) or two oxygen ions (EuCDC) and the distances Eu^{3+}–Eu^{3+} are less than 0.5 nm, which is usually stated as the limit below which exchange interactions can be observed. Considering the structural arrangements, the exchange between two Eu^{3+} ions in EuBDC should be stronger than in EuCDC because only one anion is lying between the rare earth ions. In addition the angle Eu^{3+}–O^{2-}–Eu^{3+} is almost equal to 180° in EuBDC insuring a maximum overlap between 2p(O^{2-}) and Eu^{3+} orbitals and then an exchange interaction is expected [30]. The experimental evidence of exchange or super-exchange interaction is achieved if cooperative excitation lines can be observed [31–33]. Some weak extra-lines are observed on the excitation spectrum recorded at 77 K for Eu^{3+} in EuBDC monitoring $^5D_0 \rightarrow {}^7F_2$ transition of site I at 617 nm at energy in agreement with an assignment to cooperative excitation lines; however, they are very weak and further experiments are needed to be ascribed without ambiguity to a cooperative effect.

Due to the particular structure of the studied materials, Eu^{3+} ions can also be subjected to multipolar interactions

with neighboring Eu^{3+} ions. Dimers are well isolated from others in EuCDC and direct transfer between Eu^{3+} is expected mainly between ions within a dimer. On the other hand, in EuBDC, Eu^{3+}–Eu^{3+} distance between ions within a dimer (4.716 Å) is higher than that between two ions of neighboring dimers (4.698 Å) as shown in Fig. 1; then, multipolar interactions can operate between Eu^{3+} within a dimer but also with Eu^{3+} of neighboring dimers. The non-exponential $^5D_0$ decay profile observed at short times in EuBDC, demonstrates the occurrence of energy migration. According to the structure, this migration process is expected in a restricted two-dimensional geometry.

4.1.2. Self-quenching of $^5D_1$

The decay measured for $^5D_1$ is also very short ($<1\,\mu s$). The observation of upconversion demonstrates a strong interaction between ions and a cross-relaxation process can explain the fast decay of the $^5D_1$ state in both materials. Considering levels energies the most probable scheme is the following ($^5D_1$,$^7F_0$)→($^5D_0$,$^7F_3$) although phonon assisted ($^5D_1$,$^7F_0$)→($^5D_0$,$^7F_4$) is possible at room temperature. The quenching of $^5D_1$ emission is more pronounced in EuCDC than in EuBDC probably because in this last case, the diffusion process lowers the probability to achieve cross-relaxation between two neighboring ions.

4.1.3. Self-quenching of $^5D_2$

The quenching of the $^5D_2$ state in these concentrated Eu^{3+} systems is the consequence of the strong interactions connecting Eu^{3+} within dimers and two cross-relaxation schemes are proposed to explain the experimental results. In the first one, an excited Eu^{3+} undergoes the $^5D_2$–$^5D_0$ transition while the unexcited neighbor Eu^{3+} ion undergoes the $^7F_0$–$^7F_4$ transition and/or the $^7F_1$–$^7F_4$ transition (since $^7F_1$ is populated at room temperature). A second cross-relaxation scheme ($^5D_2$,$^7F_0$)→($^5D_0$,$^7F_5$) may be also possible since the $^7F_5$ energy is not far from the $^5D_2$–$^5D_0$ energy gap. Due to the structure of both materials and to the observation of upconverted emissions, cross-relaxations are then expected.

4.2. Upconversion

The occurrence of upconverted emission with Eu^{3+} ions is not so common; on the contrary, it is obtained with other rare earth ions (Er^{3+}, Tm^{3+}, Pr^{3+}, etc.). Several reasons are at the origin of such observations. First, the particular structure of the hybrid materials under study provides the association of the RE in dimers with a fixed distance less than 0.5 nm. The coupling between these ions is expected to be significant since the spectroscopic study of Eu^{3+} in $CsCdBr_3$, an inorganic material widely studied for upconversion [30–32] and pair interaction studies [33] in which trivalent ions enter only forming [Ln^{3+}–vacancy–Ln^{3+}] pairs and [Ln^{3+}–Ln^{3+}–vacancy] dimers in a lower concentration, did not allow to observe upconversion with Eu^{3+} [34]. The weak quenching of the luminescence with increase in the Eu^{3+} concentration in both studied materials provide an opportunity to investigate the interactions between ions within a dimer.

Excited state absorption and upconversion by energy transfer give rise to anti-Stokes emission, whose intensity follows a quadratic dependence with the excitation power. The study reported in this paper is part of a wide research program on hybrid materials with different arrangements for the rare earth polyhedra (three-dimensional, two-dimensional, one-dimensional networks, isolated dimers or isolated polyhedra) and anti-Stokes emission can only be recorded for samples in which the rare earth ions are associated in dimers. For this reason, the excited state absorption from the $^5D_0$ level is excluded. Furthermore such an effect with europium has never been reported to our knowledge. The occurrence of upconversion by energy transfer in Eu^{3+} doped materials is not very common but it has already been reported in LaOCl: Eu^{3+} [25], $KLnF_4$: Eu^{3+} (Ln=Y^{3+}, Lu^{3+}) [26]. As we have stated before, cross-relaxation processes involving one ion in the $^5D_0$ state and the other in the ground state ($^7F_0$ and $^7F_{1,2}$ since they are populated at room temperature) are not possible. However, a stepwise energy transfer is likely to occur if two neighboring ions are in the $^5D_0$ state. Following this process, one ion is going on a ^7F_J state while the other is excited to a higher level. From the experimental data it is not possible to calculate which are the final states but according to the Eu^{3+} level scheme, if the final state is $^7F_0$, the others will be promoted at an energy of about 34 500 cm^{-1}, which is in the high energy part of the Eu^{3+}–$4f^6$ configuration. Then, the $^5D_1$ multiplet is populated through multiphonon relaxation from higher excited states. If the final ^7F_J state is $^7F_6$, the other ion is promoted at about 29 500 cm^{-1} as in the previous scheme, multiphonon relaxation from the final state will populate $^5D_1$.

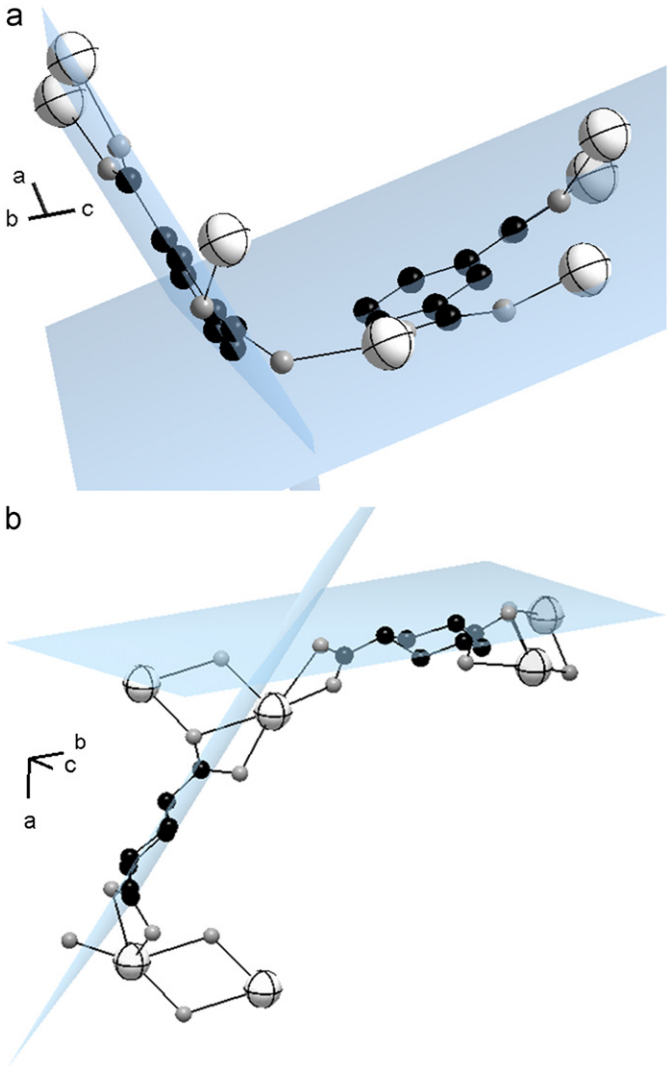

Fig. 14. Geometry of the ligand in EuBDC (a) and EuCDC (b). Europium, carbon and oxygen atoms are represented, respectively, in white (with black ellipse), black and grey. The plane around the carboxylate group is represented in blue.

4.3. Excitation spectra

In this section, we will discuss the effect of the structure and the nature of the ligand on the Eu^{3+} excitation spectrum. As presented in Fig. 4, in addition to the electronic excitation lines due to 4f–4f transitions of Eu^{3+} ion, a broad band is observed between 350 and 240 nm for EuBDC. This band was assigned to the transition between ligand states. The lack of such an excitation in EuCDC can be explained in the frame of structural considerations.

In both compounds, the rare earth is linked to the organic rings by carboxylate functions, which are in both cases in 1,3 position. Carboxylate groups are well-known for their acceptor character [34]. The central part of the ligand (1,3-benzenedicarboxylic acid for EuBDC and 1,3-cyclohexanedicarboxylic acid for EuCDC) differs from their electronic delocalization. Due to the presence of double bonds, the benzene ring exhibits a planar structure. The aromaticity of the central ring decreases from EuBDC to EuCDC and this reduces the rigidity of the structure. This first point explains the higher efficiency of the Eu^{3+} luminescence observed in EuBDC since a rigid structure reduces the non-radiative de-excitation pathways and favors donor–acceptor interactions. Taking into account the rigidity of the structure, the transfer from carboxylate and the central ring is expected to be more efficient for EuBDC than in EuCDC, which can adopt two non-planar configurations. Furthermore, from structural data, the carboxylate groups lie in planes that are almost perpendicular to the plane of the cyclohexane for EuCDC (Fig. 14(b)).

Due to the absence of coplanarity between the donor (cycle) and the neighboring acceptor carboxylate groups, the transfer of charge from the central ring to the carboxylate groups requires higher energy. In this case, the ligand states ($^1S_1$ and $^3T_1$) should lie at high energy and the $^3T_1 \rightarrow {}^1S_0$ transition should be observed beyond the detection limit of our experimental device. On the contrary in EuBDC, the acceptor carboxylate groups and the cyclic central ring are almost coplanar (5° between planes see Fig. 14(a)), a complete transfer between the π system and –COOH groups is operating, and the ligand states lie at an energy that is favorable to an efficient energy transfer to Eu^{3+} states. These considerations allow us to explain the efficient ligand–metal energy transfer in EuBDC compared to that in EuCDC.

5. Conclusion

The spectroscopic properties of Eu^{3+} ions were studied with non-selective and selective excitation in two layered hybrid materials in which the RE ions adopt a dimer structure. Energy transfer between Eu^{3+} was evidenced following laser site selective excitation in the EuBDC in which Eu^{3+} occupies two different crystallographic sites. Upconverted emission from the $^5D_1$ state is observed at room temperature after excitation in the $^5D_0$ level. Due to the structure of investigated materials, exchange, super-exchange and multipolar interactions are expected to contribute to the observed anti-Stokes emission. The main difference between optical properties of Eu^{3+} in both compounds is the ability of the host sensitization of the RE luminescence in EuBDC. The efficiency of the UV excitation due to energy transfer from the ligand state to the Eu^{3+} levels has been discussed on the basis of the ligand geometry and on the electronic delocalization within the ligand. These particular crystallographic arrangements constitute ideal lattices to study pair interactions since the quantum efficiency of fully concentrated materials is quite high. Furthermore, contrary to inorganic materials, no disorder is expected and then the inhomogenous linewidth should be very small. These materials would be probably very interesting to study coherent effects.

References

[1] S.I. Weissman, J. Chem. Phys. 10 (1942) 214.
[2] J.M. Lehn, Angew. Chem. Int. Ed. Engl. 29 (1990) 563.
[3] P.R. Selvin, J.E. Hearst, Proc. Natl. Acad. Sci. USA 91 (1994) 10024.
[4] G. Mathis, Clin. Chem. 47 (1995) 1391.
[5] J. Yuan, G. Wang, H. Kimura, K. Matsumoto, Anal. Biochem. 254 (1997) 283.
[6] T. Heyduk, Curr. Opin. Biotechnol. 13 (2002) 292.
[7] B. Juskowiak, I. Grzybowska, E. Galezowska, S. Takenaka, Anal. Chim. Acta 512 (2004) 133.
[8] L.Y. Zheng, H. Zhang, Q. Lin, G. Chuan, S. Wang, Mater. Lett. 53 (2002) 52.
[9] H. You, J. Fang, Y. Xuan, D. Ma, Mater. Sci. Eng. B 131 (2006) 252.
[10] C.G. Gameiro, C.A. Achete, R.A. Simao, E.F. da Silva Jr., P.A. Santa-Cruz, J. Alloys Compd. (2002) 344.
[11] J.-C. Bünzli, J. Alloys Compd. 408–412 (2006) 934.
[12] M. Latva, H. Takalo, V.-M. Mukkala, C. Matachescu, J.C. Rodriguez-Ubis, J. Kankare, J. Lumin. 75 (1997) 149.
[13] O.L. Malta, J. Lumin. 71 (1997) 229.
[14] C. Serre, F. Pellé, N. Gardant, G. Férey, Chem. Mater. 16 (2004) 1177.
[15] F. Millange, C. Serre, J. Marrot, N. Gardant, F. Pellé, G. Férey, J. Mater. Chem. 14 (2004) 642.
[16] C. Serre, F. Millange, C. Thouvenot, N. Gardant, F. Pellé, G. Férey, J. Mater. Chem. 14 (2004) 1540.
[17] F. Pellé, S. Surblé, C. Serre, F. Millange, G. Férey, J. Lumin. 122–123 (2007) 492.
[18] S. Surblé, C. Serre, Millange, F. Pellé, G. Férey, Solid State Sci. 7 (2005) 1074.
[19] G. Férey, Nat. Mater. 2 (2003) 136.
[20] K. Barthelet, J. Marrot, D. Riou, G. Férey, Angew. Chem.-Int. Ed. 41 (2002) 281.
[21] J.S. Seo, D. Whang, H. Lee, S.I. Jun, J. Oh, Y.J. Jeon, K. Kim, Nat. Mater. 404 (2000) 982.
[22] G. Férey, M. Latroche, C. Serre, F. Millange, T. Loiseau, A. Percheron-Guégan, Chem. Commun. (2003) 2976.
[23] Y. Qu, Y. Ke, S. Lu, R. Fan, G. Pan, J. Li, J. Mol. Struct. 7 (2005) 734.
[24] S. Surblé, C. Serre, F. Millange, F. Pellé, G. Férey, Solid State Sci. 9 (2007) 131.
[25] J. Hölsä, Chem. Phys. Lett. 112 (1984) 246.
[26] N.M. Khaidukov, X. Zhangb, J.-P. Jouart, J. Lumin. 72–74 (1997) 213.
[27] S. Pétoud, J.C. Bünzli, T. Glanzman, C. Piguet, Q. Xiang, R. Thummel, J. Lumin. (1999) 82.
[28] G.F. de Sá, O.L. Malta, C. de Mello Donegá, A.M. Simas, R.L. Longo, P.A. Santa-Cruz, E.F. da Silva Jr., Coord. Chem. Rev. 196 (2000) 165.
[29] A. Thirumurugan, S. Natarajan, J. Mater. Chem. 15 (2005) 4588.
[30] L.G. Van Uitert, L.F. Johnson, J. Chem. Phys. 44 (1966) 3514.
[31] M.A. Buijs, G. Blasse, J. Lumin. 37 (1987) 9.
[32] S. Imanaga, S. Yokono, T. Hoshina, J. Lumin. 16 (1978) 77.
[33] M. Buijs, A. Meyerink, G. Blasse, J. Lumin. 37 (1987) 9.
[34] V.F. Zolin, J. Alloys Compd. 380 (2004) 279.